Global estimates of particulate organic carbon from the surface ocean to the base of the mesopelagic

James Fox[1], Michael J. Behrenfeld[2], Kimberly H. Halsey[1], Jason R. Graff[2]

1. Department of Microbiology, Oregon State University, Corvallis, OR, United States.

2. Department of Botany and Plant Pathology, Oregon State University, Corvallis, OR, United States.

Corresponding author: James Fox (james.fox@oregonstate.edu)

Key Points:

- Float profiles of POC concentration reveal globally consistent trends in attenuation for depths below an isolume of 0.427 mol d^{-1}.
- A semi-mechanistic modeling approach can be used to accurately predict POC from the surface ocean to the base of the mesopelagic (1000m).
- The new approach enables the assessment of remineralization trends and standing stocks of POC across the global ocean.

Abstract

The gravitational settling of organic particles from the surface to the deep ocean is an important export pathway and one of the largest components of the marine biological carbon pump (BCP). The strength and efficiency of the gravitational pump is often measured using metrics reliant on reference depths and empirical formulations that parameterize the relationship between depth and flux or concentration. Here, BGC-Argo profiles were used to identify the isolume where POC concentration starts to decline, revealing attenuation trends below this isolume that are remarkably consistent across the global ocean. We developed a semi-mechanistic approach that uses observations from the first optical depth to predict POC concentration from the surface ocean to the base of the mesopelagic (1000 m), allowing assessments of spatial and temporal variability in BCP efficiencies. We find that rates of POC attenuation are high in areas of high biomass and low in areas of low biomass, supporting the view that bloom events sometimes result in a relatively weak deep biological pump characterized by low transfer efficiency to the base of the mesopelagic. Our isolume-based attenuation model was applied to satellite data to yield the first remote sensing-based estimate of integrated global POC stock of 3.02 Pg C for the upper 1000 m, with 1.27 Pg C of this global carbon stock located above the reference isolume where POC begins to attenuate.

1. Introduction

The biological carbon pump (BCP) is a collection of biological and physical processes that facilitate carbon sequestration in the deep ocean. Active transfer pathways can be physically (e.g. subduction) or biologically (e.g. mesopelagic migrators) mediated and are collectively termed particle-injection pumps (Boyd *et al.*, 2019). The biological gravitational pump (BGP) represents the amount of organic carbon that is passively transferred from sunlit surface waters to the ocean interior through particle sinking and is strongly influenced by the complexity of upper ocean food webs (Siegel *et al.*, 2014; Boyd *et al.*, 2019). Particulate organic carbon (POC) is produced by phytoplankton in the sunlit epipelagic at rates that vary spatially and temporally depending on light and nutrient availability (Westberry *et al.*, 2023). Near the base of the epipelagic zone, sunlight has been sufficiently attenuated that phytoplankton growth and particle production is outweighed by losses through remineralization and grazing, leading to decreases in POC concentration and flux (Henson *et al.*, 2012). Further remineralization of sinking particles occurs through the mesopelagic (~200 – 1000 m), resulting in a distinct vertical attenuation profile that can be measured using a variety of *in situ* approaches ranging from traps and pumps to sensors on autonomous vehicles (Baker *et al.*, 2020; Briggs *et al.*, 2020). These field observations are often combined with empirical formulations (e.g. the "Martin Curve") to estimate vertical POC profiles and calculate attenuation metrics that reflect the strength and efficiency of the BGP (Martin *et al.*, 1987; Buesseler and Boyd, 2009).

The relative change in POC concentration or flux between two depth horizons can be used to calculate the transfer efficiency from the surface to the deep ocean (Buesseler *et al.*, 2020). A lower transfer efficiency indicates faster attenuation through depth and vice versa, but the mechanisms that control BGP efficiencies are not fully understood and are a subject of debate (Armstrong *et al.*, 2001; Lam *et al.*, 2011; Henson *et al.*, 2019). The efficiency of vertical transfer controls the fate of carbon fixed at the surface, dictating whether it is partitioned into short or long-term storage pools. The transfer of carbon out of the primary production zone to the upper mesopelagic (often termed export flux) is typically viewed as short-term storage and often results in the removal of carbon from the atmosphere on timescales that span months to decades (DeVries and Weber, 2017). Long-term marine carbon storage is defined as carbon removal from the atmosphere for timescales of centuries to millennia and is estimated to occur when carbon is transported below 1000 m (IPCC 2007). The relative change in POC flux or concentration between the base of the euphotic zone and the base of the mesopelagic is referred to as flux attenuation (Passow and Carlson, 2012). The efficiency of flux attenuation varies in time and space, but it is generally observed that more than 90% of export flux is lost before the 1000 m depth threshold for long-term sequestration (Nelson *et al.*, 2002; Marsay *et al.*, 2015).

Given the importance of the BCP in modulating Earth's biogeochemical cycles, it is critical to improve our understanding of marine carbon sequestration pathways to better predict how they will change in response to climate variability (Henson *et al.*, 2019). Satellite remote sensing is a powerful tool for monitoring marine carbon stocks at global scales, but is currently limited to surface observations (Brewin *et al.*, 2023; but see Behrenfeld *et al.*, 2023). *In situ* sampling campaigns and autonomous platforms are more significantly constrained in horizontal spatial resolution, but can be used to provide detailed insight into regional sub-surface carbon cycling dynamics (Dall'Olmo *et al.*, 2016; Boyd *et al.*, 2019; Briggs *et al.*, 2020). Creating an effective framework to quantify important BCP processes at a global scale requires *in situ* observations of spatial and temporal resolution comparable to satellite data, thereby enabling effective extrapolation of surface satellite data to depth. To this end, a multifaceted approach is desirable that involves the integration of data from ship-based observations and autonomous underwater vehicles, satellite remote sensing, and numerical modeling, but programs of such scale are costly and therefore rare (Siegel *et al.*, 2016; Brewin *et al.*, 2021). As a result, there have been limited efforts to combine multi-platform observations and assess global-scale, vertically-resolved profiles of POC. To address this gap, we utilized profiling Biogeochemical-Argo (BGC-Argo) data to: (i) determine an isolume-based reference depth for the point where POC concentration begins to decline; and (ii) formulate a concentration-dependent algorithm to define attenuation trends through the water column. This semi-mechanistic approach can be used with remotely detectable properties of the first optical depth to predict POC concentrations from the surface layer to the base of the mesopelagic zone and assess spatial and temporal variations in BGP efficiencies at regional to global scales.

2. Data and Methods

2.1. Float Data and Derived Proxies

We used data collected by an array of 603 floats deployed at different times between 2010 and 2023 across several regions of the global ocean (Figure 1). Each float was equipped with a conductivity-temperature-depth sensor (SBE 41N, Seabird Scientific) and a combination bio-optical sensor (ECOTRIPLET, FLBB, MCOMS, Seabird-WetLABS). In total, these floats acquired 51,322 vertical profiles (0 – 2000 m) of salinity, temperature, pressure, chlorophyll fluorescence, and the angular scattering function at 700 nm. The raw data from each sensor were calibrated according to manufacturer guidelines by the ARGO data management team before undergoing quality control following the adjustment procedures described in Johnson et al. (2017). Chlorophyll fluorescence is then converted to chlorophyll concentration (Chl) using a linear calibration slope provided by the sensor manufacturer while backscattering is derived from the angular scattering function at 700 nm. Values of backscattering are then converted to the backscattering coefficient of particles (b_{bp_float}) by removing the scattering function of seawater using local salinity and temperature data (Zhang et al., 2009). All processed data products were downloaded from ARGO Global Data Assembly Center servers in September 2023 using the BGC-Argo-R toolbox (Cornec et al., 2021). Data flagged as poor quality were removed, along with outliers (> 98.5^{th} percentile), before profiles were interpolated to 1 m vertical resolution through the upper 1000 m. Mixed layer depth (MLD) was calculated for each float profile as the depth where density was ≥ 0.03 kg m^{-3} than the density at 10 m (de Boyer Montégut *et al.*, 2004).

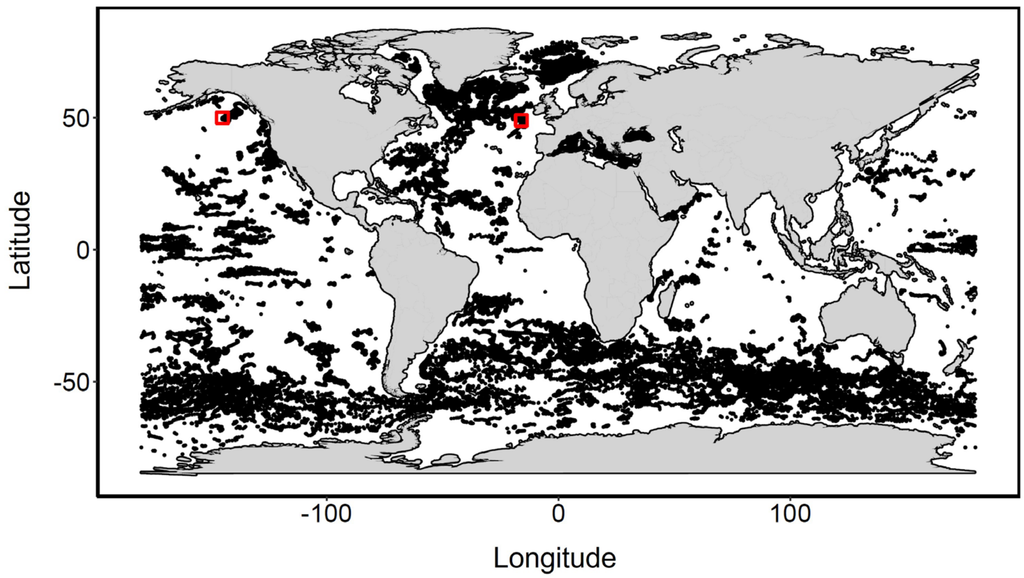

Figure 1. The global distribution of all float profiles (n = 51,322) used in this study that were collected as part of the BGC-Argo program between 2010 and 2023. Red squares show the location of sites analyzed for interannual variability.

Profiles of b_{bp_float} were smoothed with a 7-point median filter (Briggs *et al.*, 2011) before being used to estimate particulate organic carbon (POC_{float}) though depth (z) following the methods described in Gali et al. (2022):

$$POC_{float}(z) = b_{bp\_float} \cdot a, \text{ if } z \leq MLD \quad \text{Equation (1a)}$$

and

$$POC_{float}(z) = b_{bp\_float} \cdot 12100 + (a - 12100) \cdot e^{-0.00657 \cdot (z - MLD)}, \text{ if } z > MLD, \quad \text{Equation (1b)}$$

where a = 43,256 mg C m^{-3} and is the average POC/b_{bp}(700) ratio in the euphotic zone calculated using regression coefficients from several previous studies [see Table A1 in Gali et al., (2022)].

Fluorescence derived measurements of Chl were corrected for daytime non-photochemical quenching (NPQ) following Xing et al. (2012). The average Chl in the first optical depth (OD1) was then used to calculate the diffuse attenuation coefficient at 490 nm [$k_d(490)$; units = m^{-1}] following Morel & Maritorena (2001):

$$k_{\mathrm{d}}(490) = 0.0166 + 0.07242 \cdot \mathrm{Chl}^{0.68955}. \quad \text{Equation (2)}$$

Values of $k_{\mathrm{d}}(490)$ were converted to the diffuse attenuation coefficient for Photosynthetically Available Radiation (PAR), k_{PAR}, following Morel et al. (2007):

$$k_{\mathrm{PAR}} = 0.0864 + 0.884 \cdot k_{\mathrm{d}}(490) - 0.00137 \cdot [k_{\mathrm{d}}(490)]^{-1}, \text{if MLD} \leq [k_{\mathrm{d}}(490)]^{-1} \quad \text{Equation (3a)}$$

and

$$k_{\mathrm{PAR}} = 0.0665 + 0.874 \cdot k_{\mathrm{d}}(490) - 0.00121 \cdot [k_{\mathrm{d}}(490)]^{-1}, \text{if MLD} > [k_{\mathrm{d}}(490)]^{-1}. \quad \text{Equation (3b)}$$

This approach accounts for changes in spectral irradiance through depth and the subsequent impact on estimations of light attenuation. It assumes that for a homogenously mixed surface layer, attenuation coefficients for individual wavelengths in the blue-green domain (e.g. $\lambda_i \sim 443$, $\lambda_i \sim 490$, and $\lambda_i \sim 510$ nm) are only weakly dependent on the depth of that layer because these medium wavelengths typically penetrate deeper into the water column. In contrast, diffuse attenuation coefficients for the full visible spectrum (e.g. k_{PAR}) must account for the polychromatic nature of PAR and the rapid attenuation of longer wavelengths, which narrows the PAR domain at depth. As such, for a given $k_{\mathrm{d}}(490)$, k_{PAR} will decrease significantly with mixed layer depth, thus warranting different relationships for shallow, homogenous layers (Equation 3a) and deeply mixed waters (3b).

Finally, the 0.1% light depth ($\mathrm{Ez}_{0.1}$) was calculated using k_{PAR}:

$$\mathrm{Ez}_{0.1} = -\ln(0.001) / k_{\mathrm{PAR}}. \quad \text{Equation (4)}$$

2.2. Satellite Data and Derived Proxies

Ocean color products from the Moderate Resolution Imaging Spectroradiometer (MODIS) Aqua satellite used for this analysis included 9 km resolution, 8-day Chl (OCI algorithm), b_{bp} at 443 nm [$b_{bp\_sat}(443)$], derived from the Generalized Inherent Optical Property algorithm (Werdell *et al.*, 2013), the diffuse attenuation coefficient [$k_{d\_sat}(490)$], and incident PAR (PAR_0). Values of $b_{bp\_sat}(443)$ were converted to 700 nm using a power law model of the particulate backscattering coefficient spectral dependency with an exponent of -1 (Morel and Maritorena, 2001) to make them comparable with b_{bp_float}:

$$b_{bbp\_sat}(700) = b_{bbp\_sat}(443) \cdot \left(\frac{700}{443}\right)^{-1} \quad \text{Equation (5)}$$

Global estimates of MLD were calculated from salinity, temperature, and pressure data converted to density (sigma-theta) and based on daily, multi-layer products from the HYbrid Coordinate Ocean Model (HYCOM). Net primary production (NPP) for the MODIS Aqua record was estimated using the absorption-based productivity model of Silsbe et al. (2016). NPP and MLD data are available at https://sites.science.oregonstate.edu/ocean.productivity/index.php. Satellite based estimates of POC (POC_{sat}) were calculated following Equations 1a and 1b (i.e., replacing b_{bp_float} with b_{bp_sat}). Similarly, k_{PAR_sat} values were calculated using $k_{d\_sat}(490)$ and equations 3a and 3b.

2.3. Estimating the particle compensation depth

To determine an ecologically relevant reference depth corresponding to the point at which POC begins attenuating in the upper ocean, we first identified the absolute light level where POC losses to remineralization and grazing outweigh accumulation through primary production in the epipelagic zone (this isolume is henceforth referred to as the particle compensation depth, PCD). A smoothing function and a local maximum filter were first applied to each BGC-Argo profile of POC_{float} to detect sub-surface peaks in POC concentration (Supp. Figure 1). The depth of the largest peak (z_{peak}) below the mixed layer, but above the euphotic depth (defined here as the 0.01 mol d^{-1} isolume), was considered the PCD. For profiles where the MLD was deeper than the euphotic depth, z_{peak} was defined as the base of the MLD. The absolute photon flux at the PCD was then calculated as:

$$PAR_{PCD} = PAR_0 \cdot e^{(k_{PAR} \cdot z_{peak})}. \quad \text{Equation (6)}$$

Estimates of PAR_{PCD} showed a unimodal distribution with a positive skew (Supp. Figure 2), so a square root transformation was applied before the median (0.427 mol d^{-1}, Inter Quartile Range = 0.09-1.37) was taken as the global isolume for the PCD. Estimates of PAR_0 and k_{PAR} were then used to calculate the PCD for all profiles in the global dataset using this isolume:

$$z_{PCD} = -\ln\left(\frac{0.427}{PAR_0}\right) / k_{PAR}. \quad \text{Equation (7)}$$

For equation 7, the PCD was defined as MLD when $z_{PCD} \leq MLD$.

2.4. Assessing attenuation trends in POC below the PCD

Profiles of POC_{float} (e.g., Figure 2a) were used to investigate the spatial and temporal variability in attenuation trends below the PCD. First, POC_{float} data from depths shallower than the PCD were removed from all profiles in the global dataset. The remaining data of each profile were then adjusted such that the PCD depth = 0 m (e.g. $z_{norm} = z - z_{PCD}$; Figure 2b) before being fitted to a cumulative distribution function (i.e. stretched exponential model). The coefficients from all model fits were used to parameterize an algorithm to predict POC concentration below the PCD, as described in the following section.

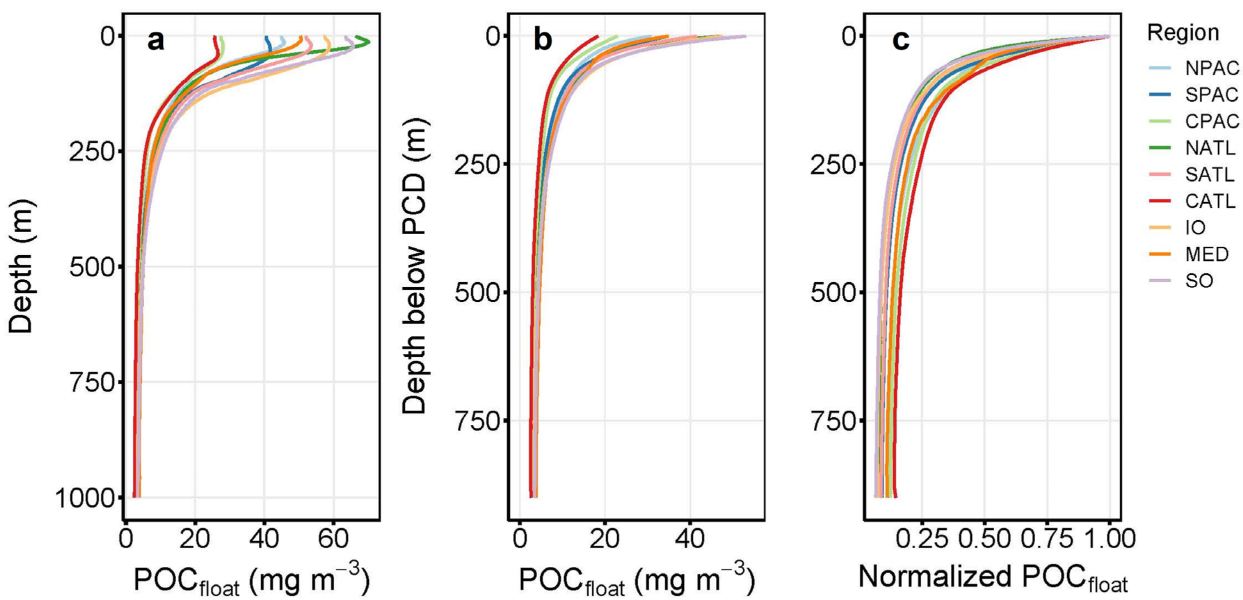

Figure 2. Regionally averaged vertical profiles of (a) particulate organic carbon derived from float observations of particulate backscatter (POC_{float}), (b) POC_{float} versus depth after removing data shallower than the particle compensation depth (PCD) and then normalizing each profile to zero depth at the PCD, and (c) data from panel b normalized to the maximum value of POC_{float} at the PCD. The regional bins are NPAC = North Pacific, NATL= North Atlantic, CPAC = Central Pacific, CATL = Central Atlantic, SPAC = South Pacific, SATL = South Atlantic, SO = Southern Ocean, IO = Indian Ocean, and MED = Mediterranean.

2.5. Modeling particulate organic carbon concentration and attenuation trends

Using the coefficients from the model fits described in section 2.4, together with surface estimates of b_{bp}, we developed an isolume-based model to predict POC concentration through the water column at 1m resolution. The first step of the approach calculates POC from the surface to the PCD using Equations 1a and 1b, and the average b_{bp} value over the first optical depth

[$b_{bp}(\mathrm{OD1})$], with the assumption that $b_{bp}(\mathrm{OD1})$ is vertically constant from the surface to the PCD. Estimates of POC below the PCD are then calculated as follows:

$$\mathrm{POC}\ (z) = \mathrm{POC_{PCD}} \cdot e^{-\left(\frac{z_{\mathrm{norm}}}{c_1}\right)^{c_2}}, \qquad \text{Equation (8)}$$

where POC at the PCD ($\mathrm{POC_{PCD}}$) is calculated using Equations 1a or 1b and $b_{bp}(\mathrm{OD1})$ when z = z_{PCD}, c_2 = 0.325, and c_1 is a concentration dependent scaling parameter calculated as:

$$c_1 = 19 + 450.29 \cdot e^{-0.0708 \cdot \mathrm{POC_{PCD}}}. \qquad \text{Equation (9)}$$

For comparison to the isolume-based attenuation model developed here, depth resolved POC concentrations were also estimated using a modified version of the 'Martin Curve' (hereafter referred to as the B20 method) where POC values at the 0.1% light depth ($\mathrm{POC_{Ez_{0.1}}}$) are fitted to a power law function following the approach described in Buesseler *et al.* (2020):

$$\mathrm{POC_{B20}}(z) = \mathrm{POC_{Ez_{0.1}}} \cdot \left(\frac{z}{\mathrm{Ez_{0.1}}}\right)^{-b}, \qquad \text{Equation (10)}$$

where *b* is the power law exponent of 0.858, and $\mathrm{POC_{Ez_{0.1}}}$ is calculated using Equation 1b when z = $\mathrm{Ez_{0.1}}$ or Equation 1a if MLD > $\mathrm{Ez_{0.1}}$.

Depth-resolved POC estimates from the isolume-based POC attenuation model (Equations 8 & 9) and the B20 method (Equation 10) were used to calculate attenuation metrics to assess the strength and efficiency of the biological carbon pump. One of these metrics was a concentration ratio (λ_{100}) which describes the change in POC between the PCD and the upper mesopelagic and is comparable to the transfer efficiency parameter derived from particle flux measurements:

$$\lambda_{100} = \frac{\mathrm{POC_{PCD+100}}}{\mathrm{POC_{PCD}}}, \qquad \text{Equation (11)}$$

where $\mathrm{POC_{PCD+100}}$ is the POC concentration 100 m below the PCD reference depth. The second attenuation metric evaluated is comparable to the flux attenuation coefficient and was calculated as the difference in POC concentration between the PCD and the base of the mesopelagic (λ_{1000}):

$$\lambda_{1000} = \frac{\mathrm{POC_{1000}}}{\mathrm{POC_{PCD}}}, \qquad \text{Equation (12)}$$

where POC_{1000} is the POC concentration at 1000 m. It is important to note that the concentration-based attenuation metrics defined here are analogous but not equivalent to traditional flux-based metrics. We nonetheless use similar terminology to emphasize the parallels, in keeping with previous studies (Lam *et al.*, 2011; Rosengard *et al.*, 2015).

Finally, global and regional depth-resolved POC were estimated using the isolume-based attenuation model (Equations 8 and 9) and the B20 method (Equation 10) with satellite retrievals of PAR, k_{PAR}, bbp, and MLD. In addition, two sites were selected to assess the interannual variability in high latitude areas of the Northeast Atlantic (49°N, 16.5°W) and the subarctic North Pacific (50ºN, 145ºW).

3. Results

3.1. Estimations of Depth Resolved POC

Regionally averaged profiles of POC_{float} from the particle compensation depth (PCD) down to 1000 m showed a two-fold range in POC concentration at the point of attenuation (Figure 2b). When these data are normalized to the POC concentration at the PCD, a consistent exponential decay profile is revealed with varying degrees of vertical compression (Figure 2c). Regions with the lowest POC concentration at the PCD (e.g. Central Pacific and Central Atlantic) typically have the most "stretched" profile, reflecting a slower rate of carbon attenuation. In contrast, high latitude regions (e.g. Southern Ocean and North Atlantic) where POC concentration is high at the PCD have steeper, more compressed profiles. The isolume-based attenuation model (red lines in Figure 3) effectively reproduces float-measured POC profiles (black lines in Figure 3) for all regions of the global ocean across all seasons (r^2 = 0.98, RMSE = 1.319; Figure 5). In comparison, the B20 method struggled to capture seasonal trends in attenuation profiles across all regions and underestimated the rate of attenuation leading to overestimates of POC through the mesopelagic (Supp. Figure 3).

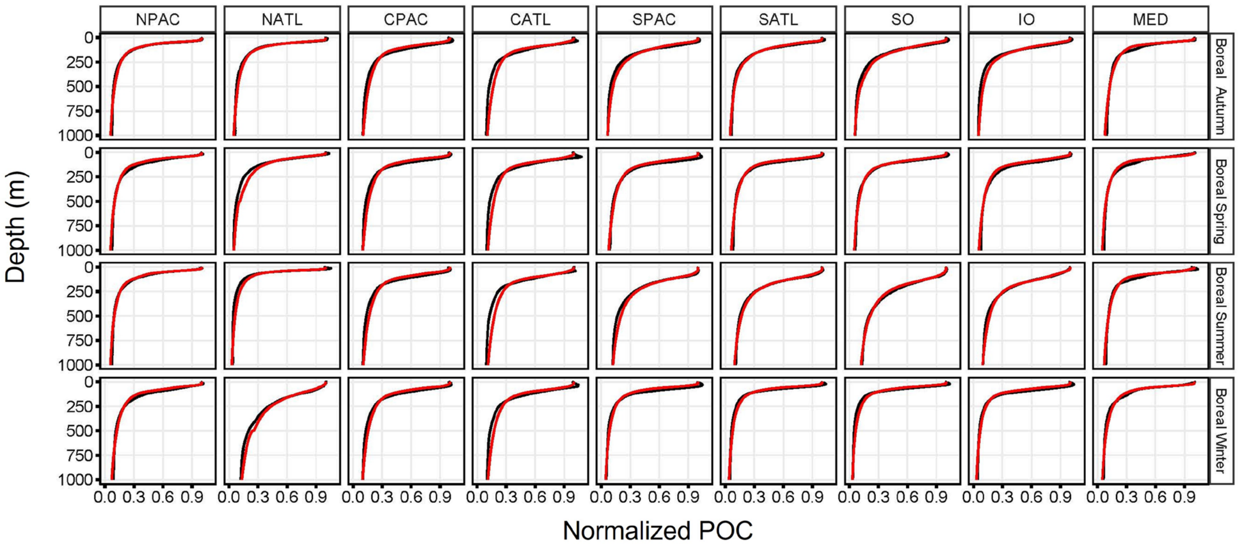

Figure 3. Seasonal variability in particulate organic carbon (POC) profiles across the global ocean. Depth resolved POC are derived from float profiles of particulate backscatter (POC_{float}, black line) and the isolume-based attenuation model approach (red line) following normalization to the POC_{float} concentration at one optical depth. The regional bins are NPAC = North Pacific, NATL= North Atlantic, CPAC = Central Pacific, CATL = Central Atlantic, SPAC = South Pacific, SATL = South Atlantic, SO = Southern Ocean, IO = Indian Ocean, and MED = Mediterranean.

Values of POC estimated using the isolume-based attenuation model and the B20 method were integrated over the top 250 m, 500 m, and 1000 m of the water column to quantify upper ocean carbon stocks. Integrated stocks predicted using the isolume-based model were averaged by region and month and showed excellent agreement with float-based observations over all depth horizons (Figure 4a). Comparisons between the isolume model and float observations averaged at finer resolution reveal the approach still performs well across all depth horizons (Figure 4b). The B20 method also showed a strong correlation with regionally averaged float observations but the slope of the regression ranged from 1.58 - 2.3, highlighting the overestimation of POC at depth due to the inability of the method to capture the correct attenuation gradient (Figure 4c).

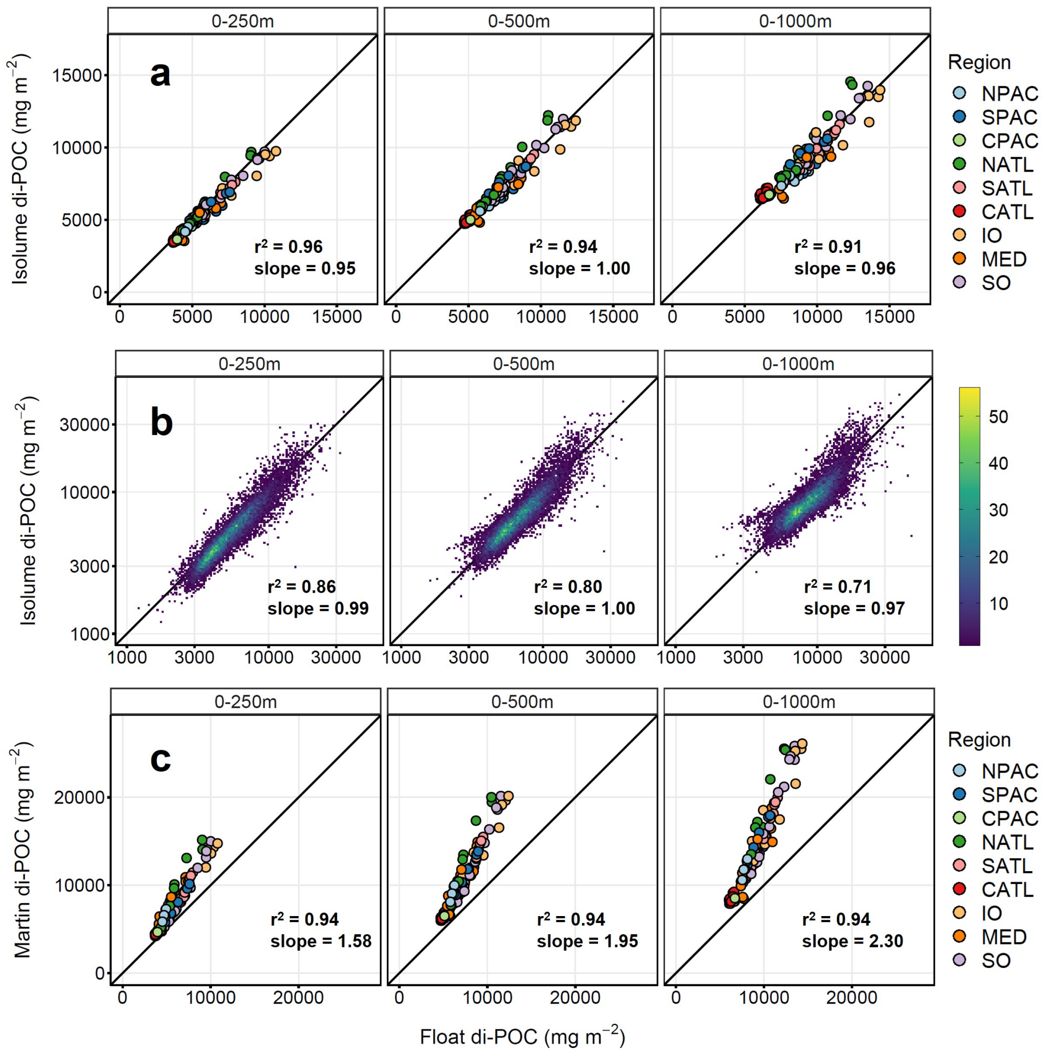

Figure 4. Particulate organic carbon (POC) values from float profiles of particulate backscatter versus model predictions integrated over the top 250m, 500m, and 1000m of the water column (left to right). (a) POC estimated using the isolume-based attenuation model and averaged by region and month (n = 108), (b) a bivariate histogram showing POC estimated using the isolume-based attenuation model averaged by float, year, region and month (n = 13,020), and (c) POC estimated using the modified Martin (B20) method and averaged by region and month (n = 108). Note the change in axis range between each plot. Color scheme for regions in (a) and (c) follows that of Figure 2.

3.2. Global Observations of POC Attenuation Metrics

Comparisons between float and model estimates of λ_{100} and λ_{1000} showed the isolume-based attenuation model performed well across the nine global ocean regions of the float database (Figure 5). Float-based measurements of POC attenuation through the upper mesopelagic reveal extensive global variability, with values ranging from ~10% to 75% (Figure 5a). Estimates of λ_{100} and λ_{1000} from the isolume-based model are generally within 10% of the float values, with slight overestimations in the Central Pacific and Central Atlantic (Figure 5). In contrast, the B20 method significantly overestimates λ_{100} in all regions due to the underestimation of POC attenuation through depth. The two different approaches are closer in performance when predicting λ_{1000}, which ranged from ~3 to 20% when calculated using float observations (Figure 5b).

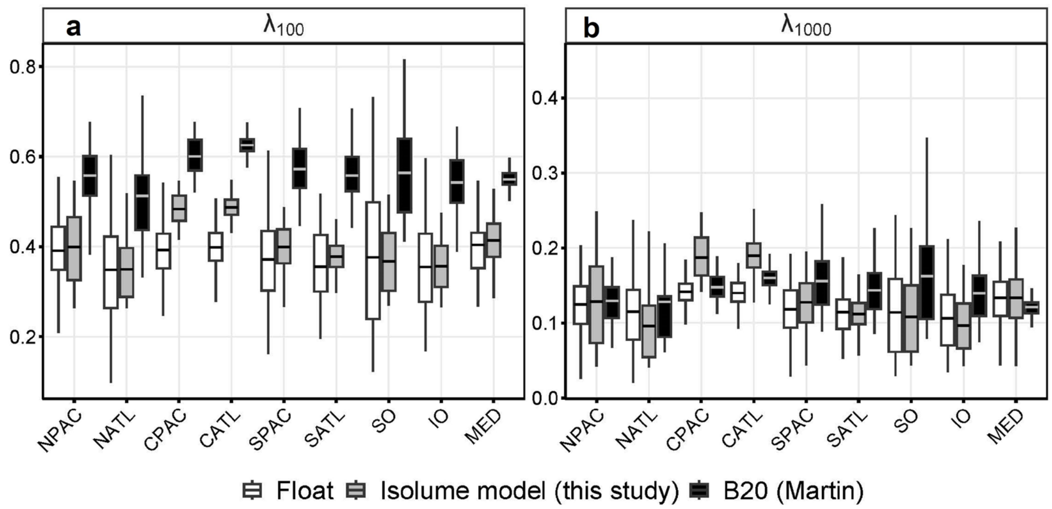

Figure 5. Values of the POC concentration gradient between the particle compensation depth (PCD) and (a) 100m below the PCD (λ_{100}), and (b) 1000 m (λ_{1000}). The estimates were made using monthly float observations (white boxes), the new isolume-based attenuation approach (grey boxes), and the modified Martin approach (B20 method; black boxes). The regional bins are the same as described in Figure 3. Note changing y-axis scales, values are unitless.

Satellite-based estimates of POC differed significantly between the PCD and the $Ez_{0.1}$, sometimes resulting in a 60% reduction in concentration between the two depth horizons (Figure 6). Global-scale attenuation metrics calculated using satellite retrievals with the B20 method and the new isolume-based attenuation model differed substantially, with the former yielding values over three-fold higher in some parts of the ocean (Figure 6i; Supp. Figure 4h-i). The isolume-based attenuation model showed more muted variability in λ_{100} estimates with most values falling between ~15-40 % (Figure 6g), and the highest efficiencies were found in the South Pacific gyre where light penetrates deepest and surface POC concentrations are incredibly low (Figure 6). High production areas, particularly areas with shallow mixed layers and high surface POC concentrations, typically had lower concentration ratios reflecting higher rates of remineralization and lower efficiencies of transfer from the surface to the mesopelagic. Annual averages of λ_{1000} largely mirrored the spatial dynamics of the λ_{100} estimates and ranged from ~3-15% (Figure 6h).

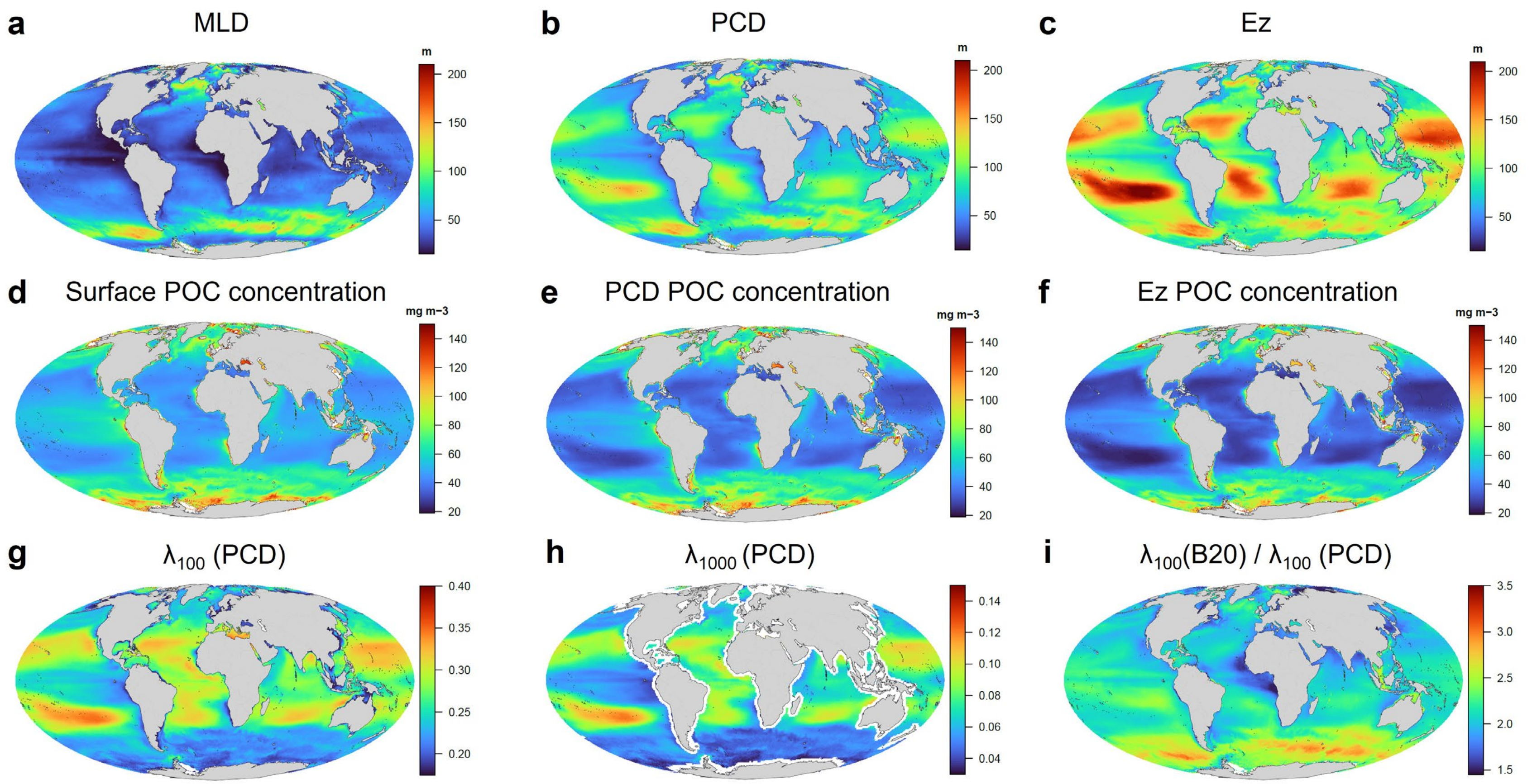

Figure 6. Satellite observations of (a) mixed layer depth (MLD, units = m), (b) the particle compensation depth (PCD, units = m), (c) the 0.1% light depth ($Ez_{0.1\%}$, units = m), (d) particulate organic carbon (POC, units mg C m^{-3}) concentration at the surface, (e) POC concentration at the PCD , (f) POC concentration at $Ez_{0.1\%}$, (g) the POC concentration ratio for the PCD and 100 m below the PCD (λ_{100}) made using the new isolume-based model, (g) the POC concentration ratio for the PCD and 1000 m (λ_{1000}) made using the new isolume-based model, (h) the difference between λ_{100} calculated using the modified Martin approach (B20) and the new isolume-based model.

3.3. Regional Interannual Variability in Carbon Dynamics

Annual cycles of NPP and POC for two Northern Hemisphere subpolar regions were assessed using satellite climatologies (Figure 7). The highest values of λ_{100} and λ_{1000} at both sites occurred in the winter months (December – February) when surface POC concentration is lowest and strong advective mixing results in deep mixed layers. Despite the ~3.5-fold change in surface POC at both sites over the annual cycle the coincident increase in attenuation rates often results in similar POC concentrations below the euphotic zone (Figure 7a and Figure 7c). Temporal trends in surface POC concentration and NPP were notably different between the two regions. In the North Atlantic, the maximum surface POC concentration occurs in spring and corresponds with high values of NPP associated with the large phytoplankton bloom event characteristic of this region (Figure 7a-b).

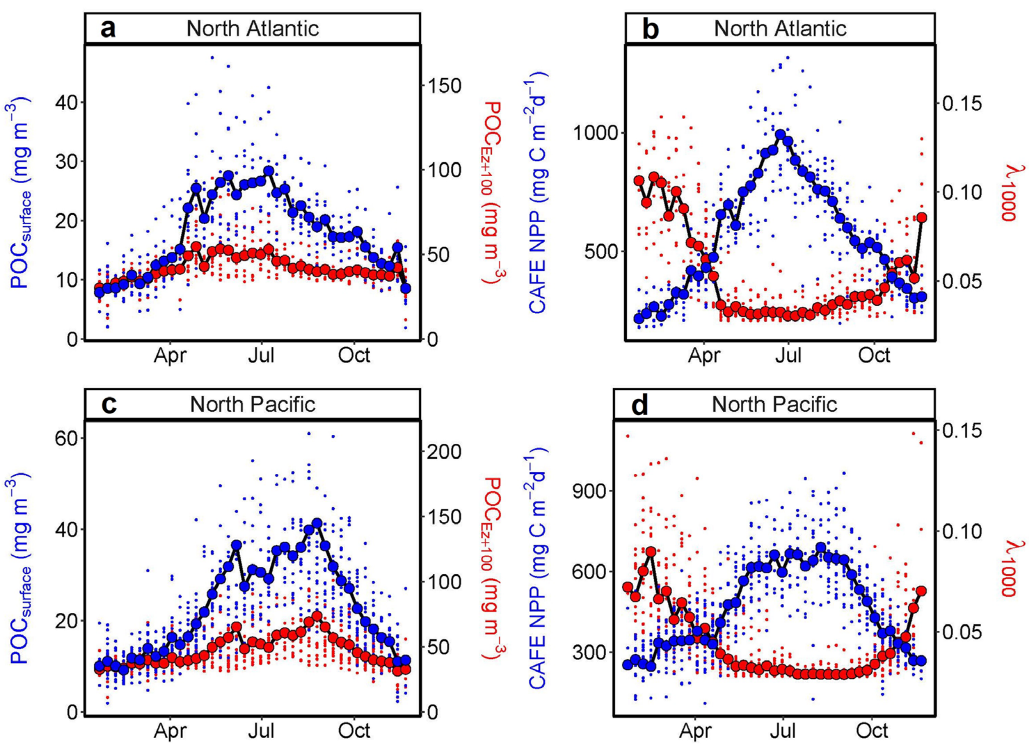

Figure 7. Climatological annual cycles of carbon stocks and rates at the Porcupine Abyssal Plain (PAP; top row) site in the Northeast Atlantic and the Ocean Station Papa (OSP; bottom row) site in the sub-arctic North Pacific, including (a) differences at PAP between surface particulate organic carbon (POC) concentration ($POC_{surface}$; large blue circles) and POC concentration 100 m below the euphotic zone (POC_{Ez+100}; large red circles) which is shown on the secondary axis, (b) net primary production (large blue circles; NPP) at PAP with the concentration gradient between the particle compensation depth (PCD) and 1000 m (λ_{1000}; large red circles) shown on the secondary axis, (c) differences at OSP between $POC_{surface}$

(large blue circles) and POC_{Ez+100} (large red circles), and (d) values of λ_{1000} and NPP at OSP. Climatologies were constructed from weekly (8 day) composites of MODIS data over a 20-year period (2003–2022) averaged over a 0.5°×0.5° pixel grid centered over the PAP and OSP sites. Small circles represent all 8-day data from the 20-year study period.

Following this spring peak, POC concentration slowly declines through summer and autumn (July – November), leading to a corresponding decrease in the rate of POC attenuation and higher values of λ_{100} and λ_{100}. In contrast, NPP and surface POC concentration both peak markedly later in the North Pacific, following a steady increase during spring and summer (April – August) (Westberry *et al.*, 2016). These peaks are immediately followed by a sharp and continuous decrease in concentration through autumn (September – November), corresponding with a lower rate of attenuation and higher concentration ratios.

4. Discussion

Satellite remote sensing is the most effective approach for monitoring marine carbon dynamics at global scales, but satellite-detected signals are largely restricted to the uppermost layer of the surface ocean (<1 optical depth) (Brewin *et al.*, 2023). Autonomous *in situ* platforms are more restricted in their horizontal spatial resolution but can provide important information on sub-surface carbon-cycling dynamics (Dall'Olmo *et al.*, 2016; Boyd *et al.*, 2019; Briggs *et al.*, 2020). Thus, surface observations of ocean color must be coupled with *in situ* observations, as well as empirical and mechanistic models, to vertically resolve the major reservoirs of marine carbon pools and understand the fluxes between different pools (Siegel *et al*., 2016). Marine POC is estimated to constitute ~80% of the organic matter exported to the deep ocean through the BCP. POC cycling in the upper 1000 m therefore plays an outsized role in defining the strength and

Table 1. POC stocks for the global ocean integrated over different depth horizons. All values are calculated using the full mission composites of MODIS AQUA data over a 20-year period (2003–2023). Coastal regions were removed from the estimates (see Figure 8). Units are Pg C.

	PACIFIC	ATLANTIC	SOUTHERN	INDIAN	Global
Surface - PCD	0.48	0.19	0.40	0.12	**1.27**
PCD – 500 m	0.50	0.20	0.32	0.13	**1.21**
500 m – 1000 m	0.23	0.10	0.12	0.06	**0.54**
Total	**1.21**	**0.49**	**0.84**	**0.31**	**3.02**

efficiency of the BCP and, in turn, is a key factor defining the magnitude of CO_2 exchange between the ocean and atmosphere. Here we introduce an isolume-based attenuation model that provides the first global estimate of POC stocks in the top 1000 m based on observations from satellite remote sensing (Figure 8; Table 1). Our method also permits estimation of POC concentrations through the water column at highly resolved resolution, thereby allowing calculation of key metrics used to assess the gravitational component of the BCP.

4.1. Predicting vertical POC using satellite observations

Remineralization of carbon through the water column is commonly parameterized as an empirical function of depth, often referred to as a 'Martin curve', which has been revised and modified in the decades since its origination (Martin *et al.*, 1987; Buesseler and Boyd, 2009, Buesseler *et al.*, 2020). Two key considerations in applying the Martin curve are the choice of reference depth from which the curve pivots and the value of the power law exponent that defines the rate of attenuation. The former is taken as the point in the water column where POC flux or concentration begins to decline, while the latter reflects the intensity of remineralization through the water column. Recently, the $Ez_{0.1\%}$ light level was proposed as a mechanistic reference depth (Buesseler et al., 2020), as opposed to the fixed point at 100 m originally used by Martin et al. (1987). In their study, Buesseler et al. (2020) found that the fixed-depth approach underestimates BCP efficiencies when the euphotic zone is shallow, and vice versa. Our results support these findings but suggest an absolute light level, or isolume,

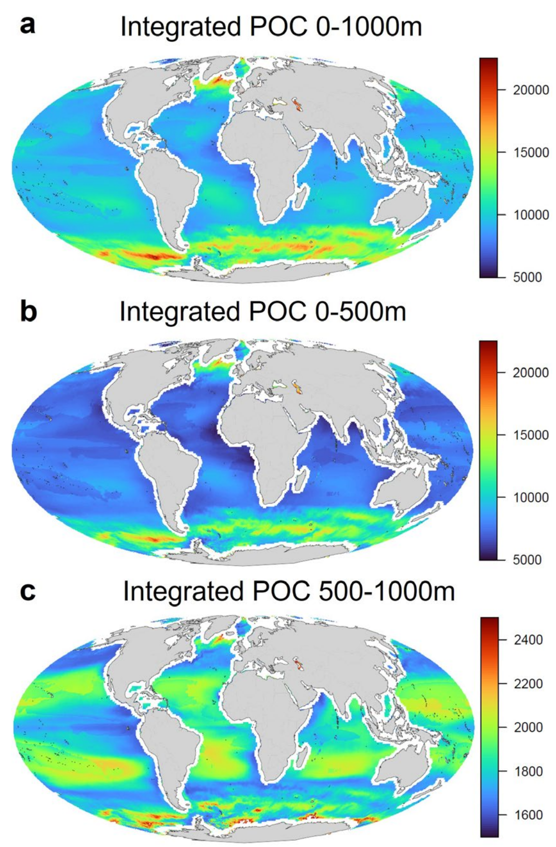

Figure 8. Global stocks of particulate organic carbon (POC) integrated over 1000 m. Input data for the new model are mission composites from MODIS AQUA at 9km resolution. Coastal waters are masked removed from the calculation of global stock estimates. Units are mg C m^{-2}.

is more suitable than a percentage when predicting the depth where particle losses outweigh gains (i.e. the PCD).

Despite the assumption that b_{bp} at OD1 will remain constant from the surface to the PCD, the isolume-based attenuation approach still predicts POC accurately through the upper water column. This result suggests that for large areas of the global ocean the concentration of POC, despite significant horizontal variability, is sufficiently homogeneous between the surface ocean and the PCD to permit extrapolation using observations from the first optical depth. One exception is the central regions of the Pacific and Atlantic where sub-surface peaks in POC result in significant variance in surface POC compared to the PCD, resulting in poorer predictions of attenuation trends. This result is consistent with a previous approach that used an empirical formulation to extrapolate satellite-derived surface observations of POC to the base of the euphotic zone (Duforêt-Gaurier *et al.*, 2010). In that study, integrated values of POC were shown to correlate well with surface values for well-mixed regions but showed a weaker relationship in stratified regions, particularly where Chl was <0.1 mg m^{-3}, such as oligotrophic regions. The weaker relationship between POC and Chl in oligotrophic regions was attributed to a deep POC maximum that coincided with the deep Chl maximum.

In addition to a fixed reference depth, the original Martin Curve formulation also used a value of 0.858 for the power law exponent, as it captured the average attention trends of the available data. Numerous studies have since shown that a fixed exponent is insufficient if the approach is to be used at a global scale (Armstrong *et al.*, 2001; Cael and Bisson, 2018). Marsay et al., (2015) suggested that temperature can be used to explain observed variability in the strength of vertical POC flux attenuation, while Lam *et al*., (2011) observed a strong positive correlation between the POC concentration at the reference depth used in the canonical Martin formulation and the power law exponent coefficient, *b* (Lam *et al*., 2011). The correlation identified by Lam et al (2011) reflects a decrease in efficiency of the BCP with increasing POC at the point of attenuation, with the highest rate of attenuation observed in high latitude regions. These results are consistent with the findings of the current study and are likely a significant factor in the marked improvement in the isolume-based attenuation model predictions through the mesopelagic compared to the B20 approach.

4.2. Defining global BCP efficiencies using the isolume-based attenuation model

The isolume-based attenuation model presented here permits the estimation of POC through the water column and can be used with satellite observations to assess global BCP efficiencies. Our results reveal the modified Martin Curve (B20 method) leads to significant overestimates of depth-resolved POC concentration and BCP efficiencies when using $Ez_{0.1}$ as a reference depth and a fixed exponent of 0.858. Other studies have used NPP or other satellite observations (e.g. phytoplankton biomass or Chl) along with food web models to predict export production and vertical carbon flux to the deep ocean (Schlitzer, 2002, 2004; Siegel *et al.*, 2014; DeVries and Weber, 2017). Those studies sought to define carbon flux, rather than concentration, and provided important steps towards understanding climate driven trends in global carbon dynamics (Wang *et al.*, 2023). The isolume-based attenuation approach presented here differs from those carbon export models in design and complexity but may benefit from it's relative simplicity. For example, one advantage of the new approach is the availability of all base input variables (e.g. MLD, k_{par}, PAR, b_{bp}) from satellite remote sensing and a lack of reliance on derived/modeled parameters such as primary production, which have been shown to significantly alter some model outputs depending on NPP model choice (Bisson *et al.*, 2018). These model features, in combination with its improved ability to estimate BGC efficiencies and POC concentration through the mesopelagic, provide new avenues to study particle cycling through the water column (Amaral *et al.*, 2022), the microbial carbon pump (Jiao *et al.*, 2010), and energy budgets of deep-sea ecosystems that rely on the export of POC from the surface.

4.3. Drivers of variability in vertical POC attenuation

Biogeochemical mechanisms defining the transfer efficiency of POC from the surface to the deep ocean through gravitational settling remain unclear but are influenced by the local composition of phytoplankton, bacteria, and zooplankton assemblages (Passow and Carlson, 2012; Turner, 2015). Recent studies show evidence supporting the hypothesis that ecosystem structure is the primary driver controlling the efficiency of the BGP, rather than other factors such as the ballasting effect of calcium carbonate and other biogenic minerals (Lam *et al.*, 2011; Henson *et al.*, 2012; Henson *et al.*, 2012; Rosengard *et al.*, 2015). A common finding across these studies is that low transfer efficiencies are typically found in high latitude regions that are often dominated by diatoms, where the proportion of NPP exported from the euphotic zone (i.e.

export efficiency) is high (Henson *et al.*, 2012). The low transfer efficiency from the surface ocean into the upper mesopelagic suggests that the POC produced in these conditions is highly labile and susceptible to remineralization, a conclusion consistent with the parameterization of the isolume-based attenuation model presented in this study. Regions where permanent or seasonal stratification give rise to phytoplankton communities dominated by smaller cells and a strong microbial loop are often characterized by a high mesopelagic transfer efficiency. *In situ* observations at these sites show higher POC concentrations deep in the mesopelagic, suggesting that the organic material exported from the surface is more resistant to remineralization at depth (Lam *et al.*, 2011). These findings are consistent with the spatial and temporal observations shown in Figure 6 and Figure 7, where high concentration ratios are generally found in permanently-stratified, oligotrophic regions while low concentration ratios are found in high latitude regions. However, we are unable to conclude whether the driver of this relationship is community composition, as suggested by Lam et al. (2011), due to the absence of taxonomic data associated with the float observations employed in our study. Our results do suggest, however, that concentration alone may be the primary driver of attenution rate [noting that while high biomass events often coincide with a high proportion of diatoms, this is not always the case (Bolaños *et al.*, 2021)].

4.4. Summary and future directions

Integrating satellite and *in situ* observations is a powerful and necessary step towards better comprehension of the ocean's biological pump. Here, we utilized BGC-Argo profiles to develop a semi-mechanistic modeling approach that employs observations from satellite remote sensing to predict POC concentrations from the ocean's surface to the base of the mesopelagic zone. The work builds on existing literature that has sought to improve empirical formulations commonly used to predict carbon cycling dynamics in the epipelagic and mesopelagic zones. The PCD isolume identified in this study offers a systematic reference depth for the point of POC attenuation which is an important step towards the accurate prediction of attenuation gradients. The new isolume based attenuation model incorporates a concentration specific scaling factor which effectively varies the attenuation gradient, with the results supported by previous studies that have assessed vertical POC distribution using *in situ* data. When combined, the PCD isolume and the algorithm for POC attenuation enables the assessment of BGP efficiencies at a global scale and the first estimation of global POC standing stock in the upper 1000 m (3.02 Pg C) made using satellite remote sensing observations. While most efforts to calculate global POC stocks using remote sensing have so far been limited to the surface layer or euphotic depth our results are incredibly similar to previous estimates. Stramska (2009) quantified POC stocks over the top 200 m using remote sensing reflectance and estimated a global average of 2.29 Pg C which is incredibly close to the prediction from this study (2.32 Pg C for surface to 200 m). A recent stock assessment over the top 1000 m, made using the Pelagic Interactions Scheme for Carbon and Ecosystem Studies (PISCES) model, also resulted in a similar value (2.6 Pg C; Galí *et al.*, 2022) to the predictions derived from our approach over the same depth horizon (3.02 Pg C; Table 1).

The enhanced ability to predict vertical profiles of POC concentration from space could open new avenues for investigating the ocean's carbon sequestration pathways. The inversion of POC concentration data recently has been shown to provide a unique approach to predicting how particle cycling rates are impacted by different biogeochemical properties in the upper ocean (Amaral et al. 2022). Combining the isolume-based attenuation model with tracer-based models could provide a new approach to predicting particle cycling dynamics in the upper ocean at a global scale. However, additional steps should also be taken to improve the accuracy of the method presented in this study. One of the simplifying assumptions in our approach is that b_{bp} at OD1 is constant to the PCD isolume which permits the calculation of POC concentration at the point of attenuation. While this assumption may hold for much of the global ocean, subsurface POC maxima in some areas of the global ocean give rise to inaccuracies in POC_{PCD} that impact predictions through depth. Significant effort has gone into predicting deep chlorophyll maxima and a similar effort to estimate the equivalent phenomena for POC will permit greater accuracy of POC concentration estimates through the mesopelagic. However, the rapid development of satellite-based lidar may soon offer ocean-observation capabilities through the water column to multiple optical depths. Other future satellite missions (e.g., NASA's Plankton, Aerosol, Cloud, ocean Ecosystem) (Werdell *et al.*, 2019) will also permit the evaluation of phytoplankton community composition which will help determine the relative impacts of biomass versus taxonomy on the POC attenuation trends.

Acknowledgments

This work was funded by NASA Grants 80NSSC21K0421 to JF and 80NSSC17KO568 to MB.

Open Research

Raw data are available from the locations described in Section 2. Processed data and code are available in the Zenodo data repository (https://doi.org/10.5281/zenodo.10775647), Github (https://github.com/jfox-osu/Data-and-scripts-for-publications), and upon request.

References

Amaral, V. J., Lam, P. J., Marchal, O., Roca-Martí, M., Fox, J. and Nelson, N. B. (2022) 'Particle cycling rates at Station P as estimated from the inversion of POC concentration data', *Elementa*. University of California Press, 10(1), pp. 1415–1428.

Armstrong, R. A., Lee, C., Hedges, J. I., Honjo, S. and Wakeham, S. G. (2001) 'A new, mechanistic model for organic carbon fluxes in the ocean based on the quantitative association of POC with ballast minerals', *Deep-Sea Research Part II: Topical Studies in Oceanography*. Elsevier Ltd, 49(1–3), pp. 219–236.

Baker, C. A., Estapa, M. L., Iversen, M., Lampitt, R. and Buesseler, K. (2020) 'Are all sediment traps created equal? An intercomparison study of carbon export methodologies at the PAP-SO site', *Progress in Oceanography*. Elsevier, 184(March), p. 102317.

Behrenfeld, M. J., Lorenzoni, L., Hu, Y., Bisson, K. M., Hostetler, C. A., Di Girolamo, P., Dionisi, D., Longo, F. and Zoffoli, S. (2023) 'Satellite Lidar Measurements as a Critical New Global Ocean Climate Record', *Remote Sensing 2023, Vol. 15, Page 5567*. Multidisciplinary Digital Publishing Institute, 15(23), p. 5567.

Bisson, K. M., Siegel, D. A., DeVries, T., Cael, B. B. and Buesseler, K. O. (2018) 'How Data Set Characteristics Influence Ocean Carbon Export Models', *Global Biogeochemical Cycles*, 32(9), pp. 1312–1328.

Bolaños, L. M., Choi, C. J., Worden, A. Z., Baetge, N., Carlson, C. A. and Giovannoni, S. (2021) 'Seasonality of the Microbial Community Composition in the North Atlantic', *Frontiers in Marine Science*. Frontiers Media SA, 8, p. 23.

Boyd, P. W., Claustre, H., Levy, M., Siegel, D. A. and Weber, T. (2019) 'Multi-faceted particle pumps drive carbon sequestration in the ocean', *Nature*, 568(7752), pp. 327–335.

de Boyer Montégut, C., Madec, G., Fischer, A. S., Lazar, A. and Iudicone, D. (2004) 'Mixed layer depth over the global ocean: An examination of profile data and a profile-based climatology', *Journal of Geophysical Research: Oceans*, 109(12), pp. 1–20.

Brewin, R. J. W., Sathyendranath, S., Kulk, G., Rio, M.-H., Concha, J. A., Woolf, D. K., *et al.* (2023) 'Ocean carbon from space: Current status and priorities for the next decade', *Earth-Science Reviews*, p. 104386.

Brewin, R. J. W., Sathyendranath, S., Platt, T., Bouman, H., Ciavatta, S., Dall'Olmo, G., Dingle, J., Groom, S., Jönsson, B., Kostadinov, T. S., Kulk, G., Laine, M., Martínez-Vicente, V., Psarra, S., Raitsos, D. E., Richardson, K., Rio, M. H., Rousseaux, C. S., Salisbury, J., Shutler, J. D. and Walker, P. (2021) 'Sensing the ocean biological carbon pump from space: A review of capabilities, concepts, research gaps and future developments', *Earth-Science Reviews*. Elsevier B.V.

Briggs, N., Dall'Olmo, G. and Claustre, H. (2020) 'Major role of particle fragmentation in regulating biological sequestration of CO2 by the oceans', *Science*. American Association for the Advancement of Science, 367(6479), pp. 791–793.

Briggs, N., Perry, M. J., Cetinić, I., Lee, C., D'Asaro, E., Gray, A. M. and Rehm, E. (2011) 'High-resolution observations of aggregate flux during a sub-polar North Atlantic spring bloom', *Deep-Sea Research Part I: Oceanographic Research Papers*, 58(10), pp. 1031–1039.

Buesseler, K. O. and Boyd, P. W. (2009) 'Shedding light on processes that control particle export and flux attenuation in the twilight zone of the open ocean', *Limnology and Oceanography*. John Wiley & Sons, Ltd, 54(4), pp. 1210–1232.

Buesseler, K. O., Boyd, P. W., Black, E. E. and Siegel, D. A. (2020) 'Metrics that matter for assessing the ocean biological carbon pump', *Proceedings of the National Academy of Sciences of the United States of America*, 117(18), pp. 9679–9687.

Cael, B. B. and Bisson, K. (2018) 'Particle flux parameterizations: Quantitative and mechanistic similarities and differences', *Frontiers in Marine Science*, 5(OCT), pp. 1–5.

Dall'Olmo, G., Dingle, J., Polimene, L., Brewin, R. J. W. and Claustre, H. (2016) 'Substantial energy input to the mesopelagic ecosystem from the seasonal mixed-layer pump', *Nature Geoscience*. Nature Publishing Group, 9(11), pp. 820–823.

DeVries, T. and Weber, T. (2017) 'The export and fate of organic matter in the ocean: New constraints from combining satellite and oceanographic tracer observations', *Global Biogeochemical Cycles*, 31(3), pp. 535–555.

Duforêt-Gaurier, L., Loisel, H., Dessailly, D., Nordkvist, K. and Alvain, S. (2010) 'Estimates of particulate organic carbon over the euphotic depth from in situ measurements. Application to satellite data over the global ocean', *Deep-Sea Research Part I: Oceanographic Research Papers*, 57(3), pp. 351–367.

Galí, M., Falls, M., Claustre, H., Aumont, O. and Bernardello, R. (2022) *Bridging the gaps between particulate backscattering measurements and modeled particulate organic carbon in the ocean*, *Biogeosciences*.

Henson, S. A., Sanders, R. and Madsen, E. (2012) 'Global patterns in efficiency of particulate organic carbon export and transfer to the deep ocean', *Global Biogeochemical Cycles*, 26(1), pp. 1–14.

Henson, S., Lampitt, R. and Johns, D. (2012) 'Variability in phytoplankton community structure in response to the North Atlantic Oscillation and implications for organic carbon flux', *Limnology and Oceanography*, 57(6), pp. 1591–1601.

Henson, S., Le Moigne, F. and Giering, S. (2019) 'Drivers of Carbon Export Efficiency in the Global Ocean', *Global Biogeochemical Cycles*, pp. 891–903.

Jiao, N., Herndl, G. J., Hansell, D. A., Benner, R., Kattner, G., Wilhelm, S. W., Kirchman, D. L., Weinbauer, M. G., Luo, T., Chen, F. and Azam, F. (2010) 'Microbial production of recalcitrant dissolved organic matter: long-term carbon storage in the global ocean', *Nature Reviews Microbiology*. Nature Publishing Group, 8(8), pp. 593–599.

Lam, P. J., Doney, S. C. and Bishop, J. K. B. (2011) 'The dynamic ocean biological pump: Insights from a global compilation of particulate organic carbon, CaCO 3, and opal concentration profiles from the mesopelagic', *Global Biogeochemical Cycles*, 25(3), pp. 1–14.

Marsay, C. M., Sanders, R. J., Henson, S. A., Pabortsava, K., Achterberg, E. P. and Lampitt, R. S. (2015) 'Attenuation of sinking particulate organic carbon flux through the mesopelagic ocean', *Proceedings of the National Academy of Sciences of the United States of America*, 112(4), pp. 1089–1094.

Martin, J. H., Knauer, G. A., Karl, D. M. and Broenkow, W. W. (1987) 'VERTEX: carbon cycling in the northeast Pacific', *Deep Sea Research Part A. Oceanographic Research Papers*, 34(2), pp. 267–285.

Morel, A., Huot, Y., Gentili, B., Werdell, P. J., Hooker, S. B. and Franz, B. A. (2007) 'Examining the consistency of products derived from various ocean color sensors in open ocean (Case 1) waters in the perspective of a multi-sensor approach', *Remote Sensing of Environment*, 111(1), pp. 69–88.

Morel, A. and Maritorena, S. (2001) 'Bio-optical properties of oceanic waters: A reappraisal', *Journal of Geophysical Research: Oceans*, 106(C4), pp. 7163–7180.

Nelson, D. M., Anderson, R. F., Barber, R. T., Brzezinski, M. A., Buesseler, K. O., Chase, Z., Collier, R. W., Dickson, M. L., François, R., Hiscock, M. R., Honjo, S., Marra, J., Martin, W. R., Sambrotto, R. N., Sayles, F. L. and Sigmon, D. E. (2002) 'Vertical budgets for organic carbon and biogenic silica in the Pacific sector of the Southern Ocean, 1996-1998', *Deep-Sea Research Part II: Topical Studies in Oceanography*, 49(9–10), pp. 1645–1674.

Passow, U. and Carlson, C. A. (2012) 'The biological pump in a high CO2 world', *Marine Ecology Progress Series*, 470(2), pp. 249–271.

Rosengard, S. Z., Lam, P. J., Balch, W. M., Auro, M. E., Pike, S., Drapeau, D. and Bowler, B. (2015) 'Carbon export and transfer to depth across the Southern Ocean Great Calcite Belt', *Biogeosciences*, 12(13), pp. 3953–3971.

Schlitzer, R. (2002) 'Carbon export fluxes in the Southern Ocean: Results from inverse modeling and comparison with satellite-based estimates', *Deep-Sea Research Part II: Topical Studies in Oceanography*, 49(9–10), pp. 1623–1644.

Schlitzer, R. (2004) ‘Export Production in the Equatorial and North Pacific Derived from Dissolved Oxygen, Nutrient and Carbon Data’, *Journal of Oceanography*, 60(1), pp. 53–62.

Siegel, D. A., Buesseler, K. O., Behrenfeld, M. J., Benitez-Nelson, C. R., Boss, E., Brzezinski, M. A., Burd, A., Carlson, C. A., D’Asaro, E. A., Doney, S. C., Perry, M. J., Stanley, R. H. R. and Steinberg, D. K. (2016) ‘Prediction of the Export and Fate of Global Ocean Net Primary Production: The EXPORTS Science Plan’, *Frontiers in Marine Science*, 3(March), pp. 1–10.

Siegel, D. A., Buesseler, K. O., Doney, S. C., Sailley, S. F., Behrenfeld, M. J. and Boyd, P. W. (2014) ‘Global assessment of ocean carbon export by combining satellite observations and food-web models’, *Global Biogeochemical Cycles*. Wiley-Blackwell, 28(3), pp. 181–196.

Stramska, M. (2009) ‘Particulate organic carbon in the global ocean derived from SeaWiFS ocean color’, *Deep-Sea Research Part I: Oceanographic Research Papers*. Elsevier, 56(9), pp. 1459–1470.

Turner, J. T. (2015) ‘Zooplankton fecal pellets, marine snow, phytodetritus and the ocean’s biological pump’, *Progress in Oceanography*. Elsevier Ltd, 130, pp. 205–248.

Wang, W.-L., Fu, W., Le Moigne, F. A. C., Letscher, R. T., Liu, Y., Tang, J. and Primeau, F. W. (2023) ‘Biological carbon pump estimate based on multidecadal hydrographic data’, *Nature*, (October 2022).

Werdell, P. J., Behrenfeld, M. J., Bontempi, P. S., Boss, E., Cairns, B., Davis, G. T., Franz, B. A., Gliese, U. B., Gorman, E. T., Hasekamp, O., Knobelspiesse, K. D., Mannino, A., Martins, J. V., McClain, C., Meister, G. and Remer, L. A. (2019) ‘The plankton, aerosol, cloud, ocean ecosystem mission status, science, advances’, *Bulletin of the American Meteorological Society*, 100(9), pp. 1775–1794.

Werdell, P. J., Franz, B. A., Bailey, S. W., Feldman, G. C., Boss, E., Brando, V. E., Dowell, M., Hirata, T., Lavender, S. J., Lee, Z. P., Loisel, H., Maritorena, S., Mélin, F., Moore, T. S., Smyth, T. J., Antoine, D., Devred, E., D’Andon, O. H. F. and Mangin, A. (2013) ‘Generalized ocean color inversion model for retrieving marine inherent optical properties’, *Applied Optics*, 52(10), pp. 2019–2037.

Westberry, T. K., Schultz, P., Behrenfeld, M. J., Dunne, J. P., Hiscock, M. R., Maritorena, S., Sarmiento, J. L. and Siegel, D. A. (2016) ‘Annual cycles of phytoplankton biomass in the subarctic Atlantic and Pacific Ocean’, *Global Biogeochemical Cycles*. Wiley-Blackwell, 30(2), pp. 175–190.

Westberry, T. K., Silsbe, G. M. and Behrenfeld, M. J. (2023) ‘Gross and net primary production in the global ocean: An ocean color remote sensing perspective’, *Earth-Science Reviews*. Elsevier B.V., 237(December 2022), p. 104322.

Xing, X., Claustre, H., Blain, S., D’Ortenzio, F., Antoine, D., Ras, J. and Guinet, C. (2012) ‘Quenching correction for in vivo chlorophyll fluorescence acquired by autonomous platforms: A case study with instrumented elephant seals in the Kerguelen region (Southern Ocean)’, *Limnology and Oceanography: Methods*, 10(JULY), pp. 483–495.